

FIG. 1: The employed experimental setup and energy level scheme. Laser beam with frequency locked to resonance with the $|e\rangle \leftrightarrow |a_2\rangle$ transition passes polarization beam splitter (PBS) and excites ^{87}Rb atoms in retro-reflected configuration. Its focus position is set precisely to coincide with the mirror plane (M_1). The photons emitted under small angle from the spatial region close to the cell back-face are polarization and frequency filtered using pairs of Glan-Thompson polarizers (G-T) and Fabry-Pérot etalons (FP). The lenses (L_1 , L_2) select and collimate the generated photons to optimize their coupling into opposite single-mode fibers (SMF) which guide them to the detection setups consisting of single-photon detectors (APDs).

nonlinear interaction medium. The cell does not contain any atomic polarization preserving coatings or buffer gas. The optical windows of the cell are antireflection coated to reduce spurious light scattering when working under small observation angles. The large ground state hyperfine splitting of ^{87}Rb isotope gives the advantage of easier spectral separation of generated photons. At the same time, employing the D_1 spectral line with only two excited states reduces off-resonant scattering from other than desired levels and simplifies the theoretical description of the SFWM process.

The requirement of using a single laser frequency suggests the double- Λ scheme as the only viable choice of energy level scheme. The respective transition strengths on D1-line lead to the excitation scheme depicted in the Fig. 1). We resonantly excite the $|e\rangle \sim 5S_{1/2}(F=2) \leftrightarrow |a_2\rangle \sim 5P_{1/2}(F=2)$ transition which results in the SFWM process starting by Raman transition from $|g\rangle \sim 5S_{1/2}(F=1)$ over $|a_1\rangle$ virtual level to $|e\rangle$ upon emission of the Stokes photon. This is followed by fast re-excitation to $|a_2\rangle$ and emission of anti-Stokes photon resonant with $|a_2\rangle \leftrightarrow |g\rangle$ transition. The virtual energy level is given by the ground hyperfine energy level splitting and ac-Stark effect from the excitation laser and therefore it is about 6.8 GHz red-detuned from the $|a_2\rangle$ state. Thermal atoms entering the excitation beam are optically pumped into the ground state $|g\rangle$. This should ideally happen before they enter the SFWM observation region, defined by the overlap between the excitation and detection spatial modes, so the uncorrelated background coming from atoms which could not undergo Stokes emission is minimized [14].

A significant advantage of our particular experimental approach is the great simplification in experimentally achieving the optimal FWM phase matching spatial arrangement. In the case of employing the double- Λ energy level scheme where frequencies of interacting photons are nearly degenerate, the correlated photons

are radiated close to exactly opposite directions. The use of the single excitation laser in retro-reflected configuration then allows for easy alignment of the whole setup without any need for auxiliary seed beams as in schemes employing several different wavelengths of absorbed and emitted photons [18, 20]. The frequency difference of $\Delta\nu_{S,AS} = 13.6$ GHz between Stokes and anti-Stokes photons together with the cancellation of the excitation laser momenta in the back-reflection excitation configuration leads to the residual phase mismatch of the realized SFWM process. This phase mismatch imposes the lower limit on the emission angle between excitation and observation directions for which the biphoton generation will be still efficient, given by the spatial length $d = c/(2\Delta\nu_{S,AS}) \sim 11$ mm corresponding to the π phase mismatch. Therefore, the observation angle should be large enough so that the excitation and observation spatial modes overlap only on the distance shorter than d . In the presented experiment, the observation angle of 2.3° together with observation and emission mode diameters of about 0.3 mm correspond to the length of the effective mode overlap of 2×3.8 mm. We consider here the effective mode overlap defined as the overlap of two transverse Gaussian mode functions higher than 50%. We note, that alternative energy level scheme on ^{87}Rb D1 line with similar efficiency can be employed by excitation of $|g\rangle \leftrightarrow |a_2\rangle$ transition with the virtual energy level in the first Raman process being then blue-detuned by about 6.8 GHz from the $|a_2\rangle$ state, however experimentally observed SFWM efficiency in this regime has been similar or slightly lower.

The excitation laser beam coming from single mode fiber (SMF) has polarization set to horizontal, that is parallel with respect to the plane defined by optical table. The beam is focused so that its waist coincides with the mirror (M_1) behind the cell with the full width at half maximum (FWHM) at the position of photon generation of 0.3 mm. This narrows the interaction area and

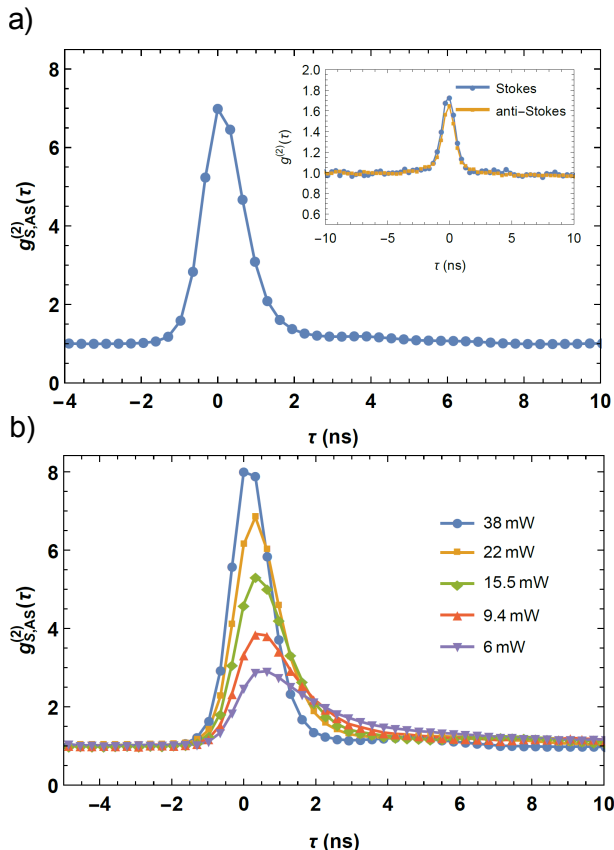


FIG. 2: a) Second-order correlation function between Stokes and anti-Stokes optical fields $g_{S,AS}^{(2)}(\tau)$. The inset shows the second-order correlations on individual Stokes $g_{S,S}^{(2)}(\tau)$ (blue circles) and anti-Stokes $g_{AS,AS}^{(2)}(\tau)$ (yellow squares) modes. The error bars are too small to be visible on the scales of the presented plots. b) Measured power dependence of the second-order correlations $g_{S,AS}^{(2)}(\tau)$.

increases the effective pump power density. The beam waist positioned at the mirror ensures that the spurious effects of beam focusing on the fulfillment of spatial phase matching conditions are minimized. In the employed small-angle scattering geometry with the angle of 2.3° between excitation and observation light directions, the Stokes and anti-Stokes fields need to be separated from the uncorrelated light scattered at strong $|e\rangle \rightarrow |a_2\rangle$ transition. We use a pair of Fabry-Pérot (FP) etalons centered at respective Stokes $|a_1\rangle \rightarrow |e\rangle$ and anti-Stokes $|a_2\rangle \rightarrow |g\rangle$ transitions. The particular setting of the FP filters thus also sets the time order of the correlations between the detected field modes. The etalons have free spectral range of about 30 GHz, transmission linewidth (FWHM) of ~ 0.6 GHz and peak transmissivity at 795 nm of 68%. Additional frequency filtering takes place in the ^{87}Rb cell itself. As can be seen in Fig. 1, the spatial alignment is set such that the point of intersection between the excitation and observation modes is close to the right end-face of the atomic cell. This allows resonant anti-Stokes photons to leave the atomic ensemble

without much losses in the direction of anti-Stokes detection setup. At the same time, far off-resonant Stokes photons are passing the whole cell without attenuation while photons resonant with $|e\rangle \rightarrow |a_2\rangle$ and $|a_2\rangle \rightarrow |g\rangle$ transitions are strongly attenuated in the same direction. In addition to uncorrelated scattering processes, the excitation beam passes a number of optical interfaces which are partially reflective and cause reflections in the directions of observed photons. We install a pair of Glan-Thompson (GT) polarizers set to transmit linear polarization orthogonal with respect to excitation beam in each observation direction to suppress the detection of these reflections. The spatial mode of emitted photons is defined by the combination of lenses (L_1 and L_2), fiber couplers, and single mode fibers (SMF), which set the spatial width of the observation region to $290 \mu\text{m}$. The overall coupling efficiency of the auxiliary aligning laser from Stokes to anti-Stokes fiber is 11.5 %, limited mostly by the finite transmission of FP cavities. Single-mode fibers in both channels are connected to detection setups consisting of single avalanche photodiodes (APDs) or Hanbury-Brown-Twiss arrangements.

III. RESULTS

The nonclassical properties of generated light fields are investigated by measurement and evaluation of normalized second-order correlation function defined as $g_{n,m}^{(2)}(t_1, t_2) = \langle a_n^\dagger(t_1)a_m^\dagger(t_2)a_m(t_2)a_n(t_1) \rangle / (\langle a_n^\dagger a_n \rangle \langle a_m^\dagger a_m \rangle)$, where a^\dagger and a are the creation and annihilation operators, n, m are field indexes and t_1, t_2 are photon detection times. The nonclassicality of generated two mode correlations can be revealed by comparison of Stokes - anti-Stokes photon correlations with the correlations measured on individual modes. For all classical states of the optical field, their mutual relation is bound by the Cauchy-Schwarz inequality (C-S) $[g_{S,AS}^{(2)}(t_1, t_2)]^2 \leq g_{S,S}^{(2)}(t_1, t_1)g_{AS,AS}^{(2)}(t_2, t_2)$, where subscripts S and AS denote measurement of second-order correlation between Stokes and anti-Stokes channels, respectively. We quantify the violation of the C-S inequality by defining the violation factor $F = [g_{S,AS}^{(2)}(\tau)]^2 / (g_{S,S}^{(2)}(0)g_{AS,AS}^{(2)}(0))$, where $\tau = t_2 - t_1$ is time between photon detections in S and AS channels.

Typical results of correlation measurement for optical depth of 1.3 and excitation beam power of 40 mW corresponding to 75 minutes of acquisition time are shown in the Fig. 2-a). The maximum of $g_{S,AS}^{(2)}(0) = (6.984 \pm 0.004)$ and the maxima of autocorrelation functions $g_{S,S}^{(2)}(0) = (1.73 \pm 0.02)$ and $g_{AS,AS}^{(2)}(0) = (1.649 \pm 0.009)$ correspond to the violation of C-S inequality by factor $F = (17.1 \pm 0.2)$. The excitation laser frequency detuning from the $|e\rangle \rightarrow |a_2\rangle$ transition has been optimized for maximization of the observed two-photon correlation $g_{S,AS}^{(2)}(0)$. The resulting optimal value corre-

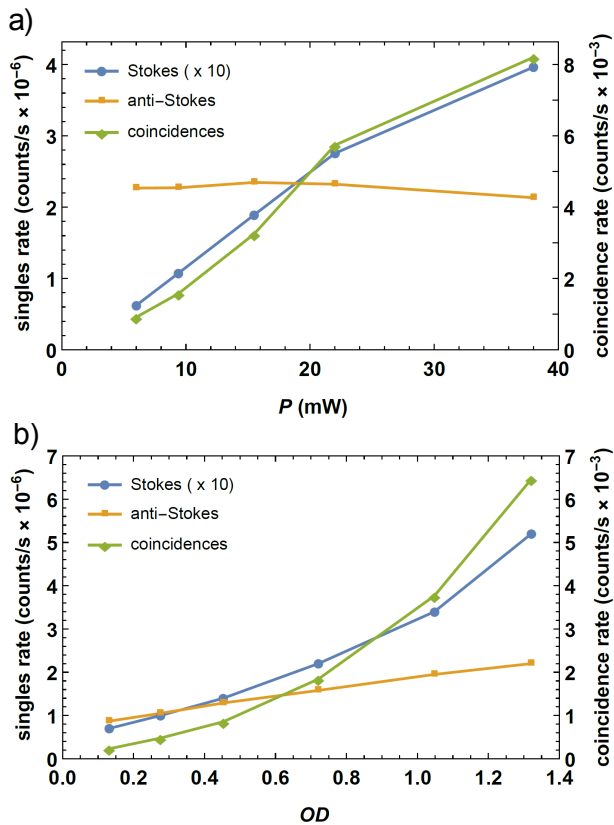


FIG. 3: The measured rates of Stokes and anti-Stokes singles and coincidences detections as a function of power a) and optical density b).

sponds to 70 MHz blue-detuned from the unperturbed $|e\rangle \rightarrow |a_2\rangle$ transition, which is much smaller than the Doppler-broadened spectral width of the atomic transition of $\sigma_D \sim 230$ MHz. This is mainly due to the requirement on the fast read-out of the stored excitation after the process of Stokes photon scattering, while the multiphoton Stokes excitations are naturally suppressed due to strongly off-resonant excitation of the Stokes transition in the presented single-laser scheme. Measurement of $g_{S,AS}^{(2)}(\tau)$ shows almost symmetric correlation peak caused by high excitation rate on the resonant $|e\rangle \rightarrow |a_2\rangle$ transition together with thermal motion of atomic cloud, which leads to broadening of the frequency bandwidth of emitted fields to scales larger than linewidths of employed Fabry-Pérot resonators. The resonators thus filter the detected time envelope to broader and symmetrical profile. The FWHM temporal width of the correlation $g_{S,AS}^{(2)}(\tau)$ has been evaluated to 1.3 ns, what is in good agreement with the theoretically expected value calculated by convolution of spectral widths of the two FP filters and specified time jitter of employed APDs of 350 ps. The peak values of autocorrelation measurements in Stokes and anti-Stokes modes suggest a partially thermal statistics of the detected light fields. The statistics of these individual modes should be generally indistin-

guishable from the one of the thermal field [21, 22], however, for the observed temporally short correlation functions, the finite time jitter of employed avalanche photodiodes decreases the correlation values substantially. Imperfect single mode nature of generated photons and small fraction of photons coming from other than desired SFWM parametric process also likely contribute to suppression of observed photon bunching. The FWHM temporal widths of correlations are equal to 1.3 ns and 1.2 ns for Stokes and anti-Stokes fields, respectively. All presented correlation functions were evaluated for 0.32 ns coincidence windows.

The detected biphoton rate within the FWHM temporal width of the S-AS correlation peak of 1.3 ns is $N_{S,AS} = (7224 \pm 85)$ pairs/s what together with Stokes and anti-Stokes count rates of $N_S = 4.8 \times 10^5$ counts/s and $N_{AS} = 18.9 \times 10^5$ counts/s corresponds to overall triggering efficiency of anti-Stokes photons of $\eta = N_{S,AS}/N_S = 1.51\%$. The rate of biphotons per 1 mW of the excitation laser power is about 180 pairs/(s mW) and the estimated biphoton rate for the triggered anti-Stokes photon bandwidth of 1 MHz is about 9.4 pairs/sec. The high ratio of anti-Stokes to Stokes count rates is caused by the detection of photons resonant with $|a_2\rangle \rightarrow |g\rangle$ transition, which do not come from the SFWM process, but are simply scattered by atoms being already in the excited state $|e\rangle$. This points to imperfect optical pumping caused by the similarity of the spatial widths of excitation and observation regions. The excitation beam diameter was not much larger than the observation area due to the limited available laser power in our experiment and, consequently, the trade-off between achievable Rabi frequency at the beam center and the efficiency of the optical pumping mechanism.

The crucial parameter influencing the efficiency and the time scale of SFWM interaction is optical power density of the exciting laser beam. Fig. 2-b) shows the second-order correlations measured for different excitation beam powers. The rest of the experimental settings is kept the same as in the correlation measurement shown in Fig. 2-a). The correlation maxima of $g_{S,AS}^{(2)}$ depend approximately linearly on the laser power, however, this dependence slowly tends to saturate for high excitation powers due to the increase of uncorrelated noise photons [14]. The measured power dependence shows, that lower excitation powers give longer excitation times on the $|e\rangle \rightarrow |a_2\rangle$ transition manifested in delayed start of the whole process. At the same time, this leaves more space for decoherence of the atomic spin wave, which becomes observable already at few nanoseconds time scales. The lower excitation power also results in longer biphoton time envelope and ability to resolve the expected exponential decay on anti-Stokes transition, as the emitted biphoton bandwidth becomes smaller than linewidths of employed FP filters. Due to the power limitations of our laser source, we were not able to further explore the scaling and seemingly emerging saturation of the power dependence. Each measured correlation curve here cor-

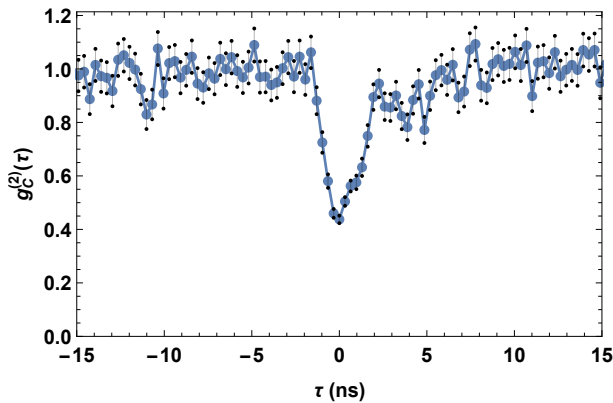


FIG. 4: Measured conditional correlation function $g_C^{(2)}(\tau)$. The error bars correspond to a single standard deviation.

responds to 5 min acquisition time. We note, that the slightly higher observed maximum of $g_{S,AS}^{(2)}(\tau)$ correlation at 38 mW excitation power compared to measurement presented in Fig. 2-a) is caused by the different spatial coupling efficiency of the biphotons into the single mode detection channels after realignment of the experimental setup.

We further characterize the observed SFWM process by measurement of the dependence of generated photon rates on the excitation laser power and atomic density while keeping the rest of the experimental settings the same as in the correlation measurement presented in Fig. 2-a). The figure 3-a) shows the expected linear dependence of far-detuned Stokes photon rates on the excitation laser power. Together with the constant emission rate of saturated anti-Stokes transition, this results in linear increase of the measured S-AS coincidences. The figure 3-b) shows the dependence of detected photon rates on optical depth set by the temperature of atomic cell. An observed quadratic increase of coincidence rate suggests that the anti-Stokes generation process is based on collective superradiant emission. Each data point in Fig. 3-a) and b) corresponds to 300 s and 60 s acquisition time, respectively.

The strong violation of the Cauchy-Schwarz inequality proves the nonclassical correlations between the two light fields, however, it does not reveal any information about the state of individual light modes conditioned on the detection of photon in the other mode. We implement the measurement of the normalized conditional second-order correlation function on the anti-Stokes field conditioned on the detection of a Stokes photon [15, 23], which can be evaluated as $g_C^{(2)}(\tau) = N_{S,AS1,AS2}(\tau)N_S / (N_{S,AS1}(0)N_{S,AS2}(\tau))$, where $N_{S,AS1,AS2}(\tau)$ is the histogram of three-photon coincidences composed of the two-fold coincidence counting event between the Stokes and anti-Stokes (AS1) detectors with fixed delay which maximizes the $g_{S,AS1}^{(2)}$ correlation and the single counting event on the second anti-Stokes detector (AS2) for various delays τ . The N_S corresponds

to the total number of triggering Stokes detections, $N_{S,AS1}$ is the total number of two-photon coincidences for the time delay corresponding again to the $g_{S,AS1}^{(2)}$ correlation maximum and $N_{S,AS2}(\tau)$ is the histogram of two-photon coincidences between the Stokes and anti-Stokes (AS2) detectors. The measured function presented in Fig. 4 shows a clear anti-bunching property of the triggered field with the minimal value of $g_C^{(2)}(0) = 0.44 \pm 0.01$. This further proves the heralded presence of nonclassical light and in addition, it suggests, that the mean photon number of the heralded state is $\langle n \rangle < 2$. The employed experimental settings are the same as in the measurements of S-AS correlations presented in Fig. 2-a) and the total acquisition time was 75 minutes. The FWHM temporal width of the triggered anti-Stokes photons was evaluated to 2.7 ns, caused mainly by the measurement of three-fold coincidences which correspond to time convolution of three photon wave-packets. The minimum value of $g_C^{(2)}(0) = 0.44 \pm 0.01$ corresponds very well to the measured correlations $g_{S,AS}^{(2)}(\tau) = 6.984 \pm 0.004$ if we consider that the detection post-selected state in the Stokes and anti-Stokes arms can be well approximated by $|1_S, 1_{AS}\rangle$ state. With this assumption, the ratio of photons coming from the desired SFWM process to uncorrelated noise photons corresponds to theoretical value of $g_C^{(2)}(0) = 2g_{AS,AS}^{(2)}(0)/g_{S,AS}^{(2)}(0) = 0.47$, where factor two corresponds to the degeneracy of detection probabilities at time delays shorter than time envelopes of detected AS photons.

IV. CONCLUSION AND OUTLOOK

We have presented the experimental realization of nonclassical light source based on the process of SFWM in warm atomic vapor and employing of only single excitation laser. The nonclassical properties of generated light fields have been proven by violation of Cauchy-Schwarz inequality by factor 17.1 ± 0.2 and by measurement of the anti-Stokes field statistics conditioned on the Stokes photon detection resulting in $g^{(2)}(0) = (0.44 \pm 0.01)$. The measured length of tunable temporal correlations on the order of several nanoseconds together with the biphoton generation rate of more than 7.2×10^3 pairs/s suggest a direct applicability of the presented source for interaction with target atomic ensembles [24–26], but also leave space for the further frequency filtering with the prospect of linewidths on the order of few MHz and with biphoton rates still applicable for investigation of storage in narrow-band atomic quantum memories [27, 28].

Compared to the recent realizations of nonclassical sources with warm atomic vapors [14, 17–20], the overall experimental scheme has been strongly simplified. Using the single excitation laser not only reduces the complexity and spatial demands of the whole experiment, but also allows for simple alignment of the spatial phase-matching in of SFWM process. Further enhancement of

the purity of generated single photons and their generation rate is expected by increasing power of the excitation laser beam, which has been limited in the current setup to 40 mW. This would allow a broader spatial width of the excitation beam at the interaction region, what would lead to better optical pumping while maintaining the required high speed of the anti-Stokes photon generation. The scheme allows for independent optimization of the Stokes and anti-Stokes transitions excitation probabilities by attenuation of the back-reflected excitation laser, what will also further improve observed nonclassical correlations [17, 20]. The presented results are likely to contribute to the development of quantum repeater based communication architectures with spatially small and technically simple single-photon sources. Further-

more, the demonstrated scheme has a strong potential for application in many experimental platforms as a technically simple source of heralded photons in close analogy to the extensively used source of broad-band photons based on spontaneous parametric down-conversion.

Acknowledgements

This work was supported by the Grant Agency of Czech Republic GB14-36681G and Palacký University IGA-PrF-2017-008. We thank Morgan Mitchell, Robert Sewell, Ferran Martin, Michał Parniak and Gabriel Hétet for valuable discussions.

-
- [1] L. M. Duan, M. D. Lukin, J. I. Cirac, and P. Zoller, “Long-distance quantum communication with atomic ensembles and linear optics,” *Nature* **414**(6862), 413-418 (2001).
- [2] N. Sangouard, C. Simon, H. de Riedmatten, and N. Gisin, “Quantum repeater based on atomic ensembles and linear optics,” *Rev. Mod. Phys.* **83**(1), 33-80 (2011).
- [3] N. Somaschi, V. Giesz, L. De Santis, J. C. Loredó, M. P. Almeida, G. Hornecker, S. L. Portalupi, T. Grange, C. Antón, J. Demory, C. Gómez, I. Sagnes, N. D. Lanzillotti-Kimura, A. Lemaitre, A. Auffeves, A. G. White, L. Lanco, and P. Senellart, “Near-optimal single-photon sources in the solid state,” *Nat. Photonics* **10**(5), 340-345 (2016).
- [4] J. Fulconis, O. Alibart, W. J. Wadsworth, P. St. J. Russell, and J. G. Rarity, “High brightness single mode source of correlated photon pairs using a photonic crystal fiber,” *Opt. Express* **13**(19), 7572-7582 (2005).
- [5] P. Farrera, G. Heinze, B. Albrecht, M. Ho, M. Chávez, C. Teo, N. Sangouard, and H. de Riedmatten, “Generation of single photons with highly tunable wave shape from a cold atomic ensemble,” *Nat. Commun.* **7**, 13556 (2016).
- [6] X. Chu, S. Götzinger, and V. Sandoghdar, “A single molecule as a high-fidelity photon gun for producing intensity-squeezed light,” *Nat. Photonics* **11**(1), 58-62 (2017).
- [7] M. Rambach, A. Nikolova, T. J. Weinhold, and A. G. White, “Sub-megahertz single photon source,” *Appl. Photonics* **1**(9), 096101 (2016).
- [8] D. B. Higginbottom, L. Slodička, G. Araneda, L. Lachman, R. Filip, M. Hennrich, and R. Blatt, “Pure single photons from a trapped atom source,” *New J. Phys.* **18**(9), 093038 (2016).
- [9] A. Kuhn, M. Hennrich, and G. Rempe, “Deterministic single-photon source for distributed quantum networking,” *Phys. Rev. Lett.* **89**(6), 067901 (2002).
- [10] R. Albrecht, A. Bommer, C. Deutsch, J. Reichel, and C. Becher, “Coupling of a single nitrogen-vacancy center in diamond to a fiber-based microcavity,” *Phys. Rev. Lett.* **110**(24), 243602 (2013).
- [11] P. Kolchín, S. Du, C. Belthangady, G. Y. Yin, and S. E. Harris, “Generation of narrow-bandwidth paired photons: use of a single driving laser,” *Phys. Rev. Lett.* **97**(11), 113602 (2006).
- [12] C. W. Chou, S. V. Polyakov, A. Kuzmich, and H. J. Kimble, “Single-photon generation from stored excitation in an atomic ensemble,” *Phys. Rev. Lett.* **92**(21), 213601 (2004).
- [13] S. Du, P. Kolchín, C. Belthangady, G. Y. Yin, and S. E. Harris, “Subnatural linewidth biphotons with controllable temporal length,” *Phys. Rev. Lett.* **100**(18), 183603 (2008).
- [14] C. Shu, P. Chen, T. K. A. Chow, L. Zhu, Y. Xiao, M.M.T. Loy, and S. Du, “Subnatural-linewidth biphotons from a Doppler-broadened hot atomic vapour cell,” *Nat. Commun.* **7**, 12783 (2016).
- [15] Y. S. Lee, S. M. Lee, H. Kim, and H. S. Moon, “Highly bright photon-pair generation in Doppler-broadened ladder-type atomic system,” *Opt. Express* **24**(24), 28083-28091 (2016).
- [16] M. W. Mitchell, C. I. Hancox, and R. Y. Chiao, “Dynamics of atom-mediated photon-photon scattering,” *Phys. Rev. A* **62**(4), 043819 (2000).
- [17] L. Zhu, X. Guo, C. Shu, H. Jeong, and S. Du, “Bright narrowband biphoton generation from a hot rubidium atomic vapor cell,” *Appl. Phys. Lett.* **110**(16), 161101 (2017).
- [18] R. T. Willis, F. E. Becerra, L. A. Orozco, and S. L. Rolston, “Correlated photon pairs generated from a warm atomic ensemble,” *Phys. Rev. A* **82**(5), 053842 (2010).
- [19] D. S. Ding, Z. Y. Zhou, B. S. Shi, X. B. Zuo, and G.-C. Guo, “Generation of non-classical correlated photon pairs via a ladder-type atomic configuration: theory and experiment,” *Opt. Express* **20**(10), 11433-11444 (2012).
- [20] Q.-F. Chen, B.-S. Shi, M. Feng, Y.-S. Zhang, and G.-C. Guo, “Non-degenerate nonclassical photon pairs in a hot atomic ensemble,” *Opt. Express* **16**(26), 21708-21713 (2008).
- [21] B. Blauensteiner, I. Herbauts, S. Bettelli, A. Poppe, and H. Hübel, “Photon bunching in parametric down-conversion with continuous-wave excitation,” *Phys. Rev. A* **79**(6), 063846 (2009).
- [22] B. Yurke and M. Potasek, “Obtainment of thermal noise from a pure quantum state,” *Phys. Rev. A*, **36**(7), 3464-3466 (1987).
- [23] P. Grangier, G. Roger, and A. Aspect, “Experimental

- evidence for a photon anticorrelation effect on a beam splitter: a new light on single-photon interferences,” *Europhys. Lett.* **1**(4), 173 (1986).
- [24] N. Mercadier, W. Guerin, M. Chevrollier, and R. Kaiser, “Lévy flights of photons in hot atomic vapours,” *Nat. Phys.* **5**(8), 602 - 605 (2009).
- [25] K. T. Kaczmarek, P. M. Ledingham, B. Brecht, S. E. Thomas, G. S. Thekkadath, O. Lazo-Arjona, J. H. D. Munns, E. Poem, A. Feizpour, D. J. Saunders, J. Nunn, and I. A. Walmsley, “A room-temperature noise-free quantum memory for broadband light,” [arXiv:1704.00013](https://arxiv.org/abs/1704.00013) (2017).
- [26] J. Wolters, G. Buser, A. Horsley, L. Beguin, A. Jöckel, J.-P. Jahn, R. J. Warburton, and P. Treutlein, “Simple atomic quantum memory suitable for semiconductor quantum dot single photons,” *Phys. Rev. Lett.* **119**(6), 060502 (2017).
- [27] M. D. Eisaman, A. André, F. Massou, M. Fleischhauer, A. S. Zibrov, and M. D. Lukin, “Electromagnetically induced transparency with tunable single-photon pulses,” *Nature* **438**(7069), 837-841 (2005).
- [28] I. Novikova, R. L. Walsworth, and Y. Xiao, “EIT-based slow and stored light in warm atoms,” *Laser Photonics Rev.* **6**(3), 333-353 (2012).